

Effective-range approximations for resonant scattering of cold atoms

Caroline L. Blackley,¹ Paul S. Julienne,² and Jeremy M. Hutson¹

¹*Joint Quantum Centre (JQC) Durham/Newcastle, Department of Chemistry,
Durham University, South Road, Durham, DH1 3LE, United Kingdom*

²*Joint Quantum Institute, University of Maryland and NIST, College Park, Maryland, 20742, USA*

(Dated: November 14, 2021)

Studies of cold atom collisions and few-body interactions often require the energy dependence of the scattering phase shift, which is usually expressed in terms of an effective-range expansion. We use accurate coupled-channel calculations on ⁶Li, ³⁹K and ¹³³Cs to explore the behavior of the effective range in the vicinity of both broad and narrow Feshbach resonances. We show that commonly used expressions for the effective range break down dramatically for narrow resonances and near the zero-crossings of broad resonances. We present an alternative parametrization of the effective range that is accurate through both the pole and the zero-crossing for both broad and narrow resonances. However, the effective range expansion can still fail at quite low collision energies, particularly around narrow resonances. We demonstrate that an analytical form of an energy and magnetic field-dependent phase shift, based on multichannel quantum defect theory, gives accurate results for the energy-dependent scattering length.

I. INTRODUCTION

The study of trapped samples of ultracold atomic gases is an extremely fruitful area of experimental and theoretical research. It includes studies of Bose-Einstein condensation (BEC) of bosonic species [1–4], the crossover between the BEC and Bardeen-Cooper-Schrieffer regimes of fermionic species [5–7], the production of ultracold polar molecules [8–10], the manipulation of atoms in optical lattices [11, 12], and the study of Efimov physics in few-body systems [13–16]. The theory of such phenomena has been greatly simplified by the ability to characterize the zero-energy interaction of two atoms in terms of the *s*-wave scattering length *a*. For many species, nearly any desirable value *a*(*B*) can be obtained by tuning a magnetic field *B* near the pole position *B*₀ of a threshold scattering resonance known as a Feshbach resonance. The scattering length is approximately related to the magnetic field by the formula [17]

$$a(B) = a_{\text{bg}} \left(1 - \frac{\Delta}{B - B_0} \right), \quad (1)$$

where Δ is the width of the resonance and a_{bg} is the background scattering length far from resonance.

The parametrization of low-energy interactions in terms of *a*(*B*) allows the detailed chemical interaction between two ultracold atoms in the limit of zero collision kinetic energy $E \rightarrow 0$ to be replaced by a zero-range Fermi pseudo-potential whose strength is proportional to *a*(*B*). However, as experimental probes of ultracold systems become more powerful and sophisticated, the variation of atomic interactions as a function of energy away from exactly $E = 0$ must be considered and understood. The usual way to describe the variation with energy of the near-threshold *s*-wave scattering phase shift $\eta(E)$ is to use an effective-range expansion at small collision momentum $\hbar k$, where $E = \hbar^2 k^2 / (2\mu)$ and μ is the reduced

mass of the two atoms [18, 19],

$$k \cot \eta(E) = -\frac{1}{a_0} + \frac{1}{2} r_{\text{eff}} k^2 + \dots, \quad (2)$$

where the parameter r_{eff} is called the effective range and a_0 is the zero-energy scattering length. We prefer a modified way of writing this expression and define the energy-dependent scattering length *a*(*E*) by [20],

$$a(E) = -\frac{\tan \eta(E)}{k} = \frac{1}{ik} \frac{1 - S(E)}{1 + S(E)}, \quad (3)$$

where $S = e^{2i\eta}$ is the diagonal element of the unitary *S*-matrix for the threshold channel in question. With this formulation, both $\eta(E)$ and *a*(*E*) are real when only elastic scattering is possible but become complex in the presence of inelasticity. Eq. (2) becomes

$$a(E)^{-1} = a_0^{-1} - \frac{1}{2} r_{\text{eff}} k^2 + \dots, \quad (4a)$$

or

$$a(E) = a_0 + \frac{1}{2} r_{\text{eff}} a_0^2 k^2 + \dots \quad (4b)$$

Far from a pole or a zero-crossing in $a_0(B)$, finite-difference equations based on either of these relationships may be used to evaluate r_{eff} . However, those based on (4a) are numerically unstable near a zero-crossing and those based on (4b) are numerically unstable near a pole.

Effective-range expansions have been invoked to include the role of collisions at finite energy in few-body phenomena [21–25] and to correct for the zero-point energy in optical lattice physics [26]. The energy-variation of the phase shift is needed to obtain the contribution of two-body collisions to low-energy partition functions and thermodynamic properties of cold gases [27]. The effective range is known to vary around Feshbach resonances [14, 25, 28–31], but there has been no in-depth numerical study of the behavior of $\eta(E)$, *a*(*E*) and r_{eff} as *B* is

tuned across Feshbach resonances of different types. In the present work we use accurate coupled-channels calculations to explore this numerically for both broad and narrow Feshbach resonances. Our calculations demonstrate that the effective-range expansion can fail in some circumstances for low-energy atomic collisions and also elucidate the range of applicability of simple approximations that have been developed to relate the effective range to the scattering length, given the form of the long-range potential [32]. We also present an approach based on multichannel quantum defect theory (MQDT) [32], which gives an analytic form for the energy-dependence of the phase shift that applies even when the effective-range expansion breaks down. We will demonstrate that this analytic representation gives excellent agreement with coupled-channels calculations for both broad and narrow resonances.

We choose to study resonances in ${}^6\text{Li}$, ${}^{133}\text{Cs}$ and ${}^{39}\text{K}$, in their lowest possible s -wave collision channels, all of which are important in studies of Efimov physics [14–16, 33–38]. The interaction potentials used in the coupled-channels calculations are those of Zürn *et al.* [39] for ${}^6\text{Li}$, Berninger *et al.* [16, 40] for ${}^{133}\text{Cs}$, and Falke *et al.* [41] for ${}^{39}\text{K}$. The atomic hyperfine/Zeeman states are labelled using Roman letters a,b,c, etc., in increasing order of energy.

The structure of the paper is as follows: Section II describes effective-range theory, including the magnetic field dependence of the effective range; Section III discusses the limits of the effective-range expansion; Section IV describes the MQDT approach to the energy-dependent scattering length; Section V details the effectiveness of this new approach and Section VI concludes with a summary of the applicability and accuracy of both effective-range theory and the MQDT-based approach.

II. BEHAVIOR OF THE EFFECTIVE RANGE NEAR A FESHBACH RESONANCE

In this section we analyse the behavior of the effective range in the vicinity of Feshbach resonances of different types. A magnetically tunable resonance can be classified as broad or narrow, based on the parameter s_{res} [42],

$$s_{\text{res}} = \frac{a_{\text{bg}}}{\bar{a}} \frac{\delta\mu\Delta}{\bar{E}}, \quad (5)$$

where a_{bg} is the ‘‘local’’ background scattering length, $\delta\mu$ is the difference between the magnetic moment of the bare bound state and the magnetic moment of the separated atoms, and Δ is the width of the resonance. The length and energy scales \bar{a} and \bar{E} are as defined by Gribakin and Flambaum [43],

$$\bar{a} = \frac{2\pi}{\Gamma(1/4)^2} \left(\frac{2\mu C_6}{\hbar^2} \right)^{1/4} \quad (6)$$

$$\bar{E} = \frac{\hbar^2}{2\mu\bar{a}^2}. \quad (7)$$

Using these scalings allow us to define dimensionless length and energy parameters, a/\bar{a} and E/\bar{E} , respectively. Resonances with $s_{\text{res}} > 1$ are referred to as broad resonances, whilst those with $s_{\text{res}} < 1$ are narrow resonances.

The effective-range expansion is the leading term in a Taylor series and breaks down at ‘high’ energies. However, in the present work it is always valid up to at least $E/k_{\text{B}} = 50$ nK. We therefore obtain r_{eff} at each magnetic field by performing coupled-channels calculations at 1 pK and 10 nK and fitting the resulting values of $a(E)$ from Eq. (3) to either Eq. (4a) or Eq. (4b). The coupled-channels calculations are performed using the MOLSCAT package [44], adapted to handle collisions in external fields [45]. Calculations are carried out with a fixed-step log-derivative propagator [46] at short range and a variable-step Airy propagator [47] at long range. The wavefunctions are matched to their long-range solutions, the Ricatti-Bessel functions, to find the S-matrix elements; these are related to the energy-dependent scattering length and phase shift by Eq. (3).

Gao [29] and Flambaum *et al.* [30] have developed an approximate formula relating r_{eff} to a , based on the case of single-channel scattering with an R^{-6} potential,

$$r_{\text{eff}} \approx \left(\frac{\Gamma(1/4)^4}{6\pi^2} \right) \bar{a} \left[1 - 2 \left(\frac{\bar{a}}{a_0} \right) + 2 \left(\frac{\bar{a}}{a_0} \right)^2 \right]. \quad (8)$$

We show below that this formula works well near the pole of a broad resonance, but may break down around a zero-crossing. In particular, (8) predicts that r_{eff} is always positive, which is not in fact the case. For narrow resonances, we demonstrate that the parabolic dependence on $1/a_0$ is retained, but quite different coefficients are required.

To contrast the behavior of the effective range across broad and narrow resonances, we consider ${}^6\text{Li}$ in its lowest (ab) s -wave scattering channel. Using an $L = 0$ (s -only) basis set, the scattering length for this channel has only two resonances at fields below 1000 G, one broad near 832 G ($\Delta = -262$ G) and the other narrow near 543.40 G ($\Delta = 0.10$ G) [39]. The system is somewhat unusual because the narrow resonance is close to the zero-crossing of the broad resonance. However, as the spacing in magnetic field between the two features is several orders of magnitude greater than the width of the narrow resonance, the overall behavior of the two features is still distinct.

The scattering length $a(B)$ and effective range $r_{\text{eff}}(B)$ for ${}^6\text{Li}$ are shown in Figure 1(a) between 200 and 1000 G. For the wide resonance, the effective range is a smooth function of magnetic field except near the zero-crossing in $a_0(B)$ close to 527 G, where it diverges to negative values. This may be contrasted with the behavior of Gao’s formula (8), also shown in Fig. 1, which diverges to positive values. The quantity $r_{\text{eff}}a_0^2$, shown in Fig. 1(c) as a function of field, is continuous through the zero-crossing, but naturally diverges at the resonance pole,

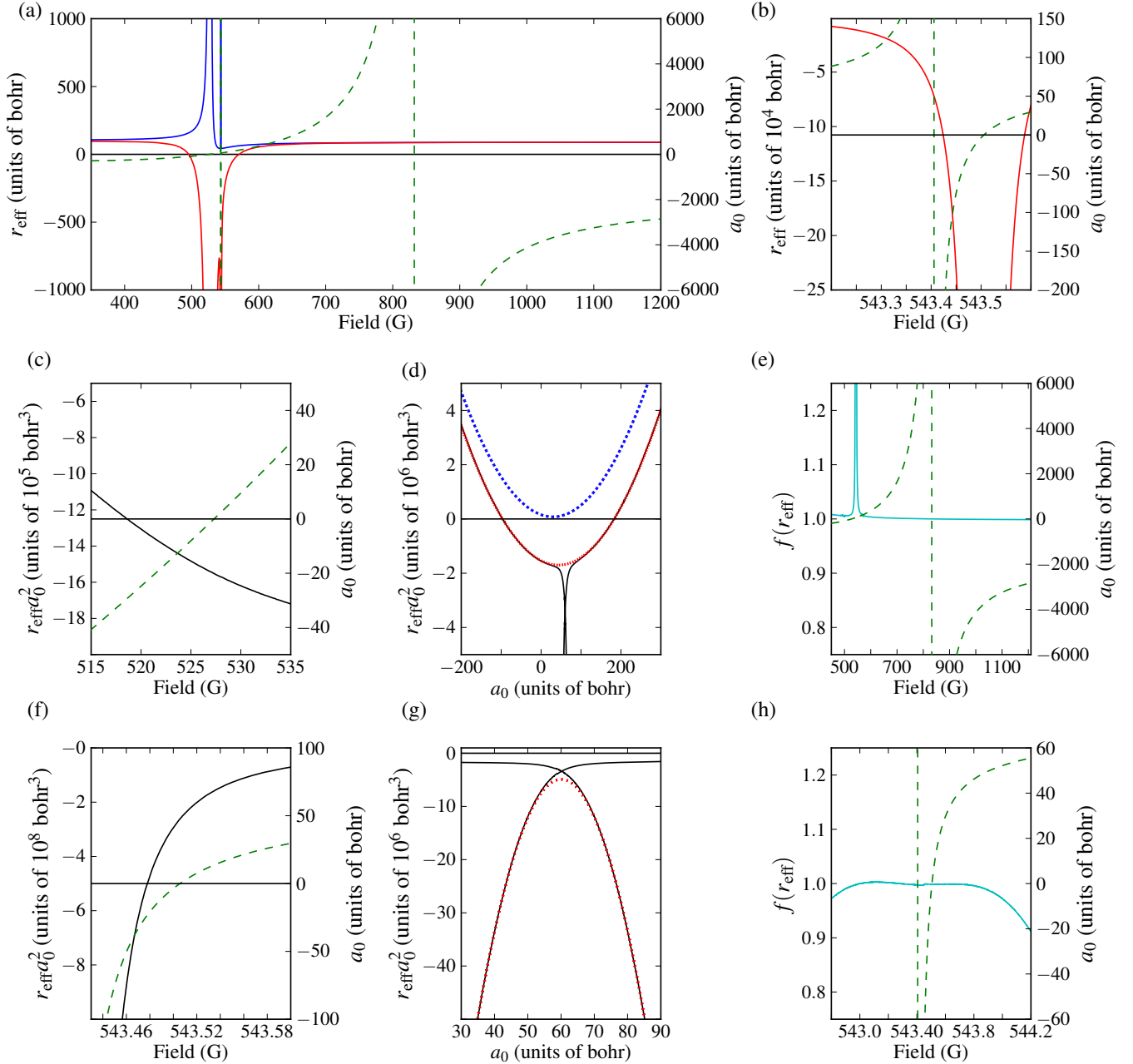


FIG. 1. (a) The field-dependent effective range for the ab channel of ${}^6\text{Li}$ from coupled-channel calculations (red solid or light gray) and as calculated from Eq. (8) (blue solid or dark gray). The zero-energy s-wave scattering length is also shown (green dashed). (b) An expanded view of (a) showing the narrow resonance at 543.40 G. (c) and (f) The quantity $r_{\text{eff}}a_0^2$ (black solid), which is a smoothly varying function of magnetic field through the zero-crossing of a_0 (green dashed) for both the wide resonance (c) and the narrow resonance (f). (d) The quantity $r_{\text{eff}}a_0^2$ (black), which is parabolic as a function of a_0 across the width of the wide resonance, except around the narrow resonance. The red dotted line shows the parabola $v + r_0(a_0 - a_{\text{ext}})^2$ fitted to the coupled-channel results, while the blue dotted (upper) line shows the corresponding parabola from Eq. (9). (e) The function $f(r_{\text{eff}})$ of Eq. (11) (cyan), with parameters appropriate for the wide resonance, which is constant across the width of the wide resonance in a_0 (green dashed) except around the narrow resonance. (g) the quantity $r_{\text{eff}}a_0^2$ (black solid), which is parabolic as a function of a_0 across the width of the narrow resonance; the red dotted line shows the parabola $v + r_0(a_0 - a_{\text{ext}})^2$ fitted to the coupled-channel results. (h) The function $f(r_{\text{eff}})$ of Eq. (11) (cyan), with parameters appropriate for the narrow resonance, which is constant across the width of the narrow resonance in a_0 (green dashed).

where r_{eff} itself does not. As shown in Fig. 1(d), it is close to parabolic as a function of a_0 , except close to the narrow resonance. However, the parabola dips below zero between $a_0 = 183$ and -96 bohr, accounting for the fact that r_{eff} is negative in this region. The corresponding parabola from Gao's formula,

$$r_{\text{eff}}a_0^2 \approx \left(\frac{\Gamma(1/4)^4}{6\pi^2} \right) [\bar{a}^3 + \bar{a}(a_0 - \bar{a})^2], \quad (9)$$

is also shown in Fig. 1(d). It is similar to the true parabola but is offset from it and is positive everywhere, with a minimum value of $\bar{a}^3\Gamma(1/4)^4/6\pi^2 = 77840$ bohr³ at $a_0 = \bar{a}$.

The values of $r_{\text{eff}}a_0^2$ from coupled-channel calculations may be fitted to a parabola

$$r_{\text{eff}}a_0^2 = v + r_0(a_0 - a_{\text{ext}})^2, \quad (10)$$

with parameters given in Table I. By construction, r_0 is the value of r_{eff} at the resonance pole. The quantity

$$f(r_{\text{eff}}) = \frac{r_{\text{eff}}a_0^2}{v + r_0(a_0 - a_{\text{ext}})^2} \quad (11)$$

is almost constant across the whole width of the broad resonance, except close to the narrow resonance, as shown in Fig. 1(e).

In the narrow-resonance region, the effective range varies very fast with magnetic field even very close to the pole, as shown in Fig. 1(b). An expanded view of $r_{\text{eff}}a_0^2$ in this region is shown in Fig. 1(g). It is clear that $r_{\text{eff}}a_0^2$ is actually double-valued as a function of a_0 : the narrow resonance contributes a second near-parabolic feature, but it has completely different parameters from the parabola for the broad resonance. We have fitted a parabola of the same form to points away from the region around $a_0 = 59$ bohr, where the narrow resonance reaches its background scattering length and rejoins with the wide resonance, and the resulting curve is shown in Fig. 1(g). The parameters of the parabola for the narrow resonance, also given in Table I, bear no resemblance to those from Gao's formula (9).

Petrov [48] and Bruun *et al.* [49] introduced a parameter R^* , defined as

$$R^* = \frac{\hbar^2}{2\mu a_{\text{bg}} \Delta \delta \mu} = \frac{\bar{a}}{s_{\text{res}}}. \quad (12)$$

For narrow resonances, this is large and positive and is related to the effective range at the pole by $R^* \approx -r_0/2$. The values obtained from this expression are included in Table I; it may be seen that R^* is within about 4% of $-r_0/2$ for the narrow resonance in ⁶Li, but (as expected) bears no resemblance to it for the broad resonance.

To explore further the behavior of the effective range around narrow resonances, we have carried out additional calculations on the resonances at 744.93 G in the aa channel of ³⁹K and at 226.73 G in the aa channel of Cs. The ³⁹K resonance is caused by an $L = 0$ bound

state, whereas the Cs resonance is caused by an $L = 2$ bound state. The quantity $r_{\text{eff}}a_0^2$ was again found to be close to parabolic in each case, with parameters given in Table I. It may be seen that r_0 and v may have the same or different signs; when they are different, r_{eff} diverges at the zero-crossing with the opposite sign to its value at the pole. For narrow resonances, the position of the extremum in $r_{\text{eff}}a_0^2$, a_{ext} , is typically close to a_{bg} . This is consistent with the expression given by Zinner and Thogerson [28] for r_{eff} in the vicinity of a narrow resonance, $r_{\text{eff}} = r_0(1 - a_{\text{bg}}/a_0)^2$. However, this expression gives $r_{\text{eff}} = 0$ far from resonance. If we add a ‘‘background’’ effective range $r_{\text{eff,bg}}$, the resulting parabola for $r_{\text{eff}}a_0^2$ is of the form of Eq. (10), with

$$a_{\text{ext}} = a_{\text{bg}}(1 - r_{\text{eff,bg}}/r_0) \quad (13a)$$

and

$$v = a_{\text{bg}}a_{\text{ext}}r_{\text{eff,bg}}. \quad (13b)$$

For resonances that are not very narrow, this effect can make a_{ext} significantly different from a_{bg} , as seen for the Cs resonance at 226.73 G in Table I. For the isolated resonances in ³⁹K and Cs, Gao's formula (8), evaluated for $a_0 = a_{\text{bg}}$, gives $r_{\text{eff,bg}}$ and hence v and a_{ext} within 10% of the values in Table I. Eq. (10), together with parameters from Eqs. (8), (12) and (13), thus provides a useful approximate expression for r_{eff} in the vicinity of an isolated narrow resonance that does not require coupled-channel calculations.

III. LIMITATIONS OF THE EFFECTIVE-RANGE EXPANSION

In this section, we assess the range of energies over which the effective-range expansion provides an accurate representation of the energy-dependent scattering length. We consider the same 4 resonances as in Section II, at collision energies ranging from 1 nK to 1 mK. For each resonance, we calculate the energy-dependent phase shift at multiple magnetic fields around the zero-energy pole position. For resonances at the lowest atomic threshold, the state responsible for the resonance is always bound on the low-field side of the zero-energy resonance pole. We therefore calculate $\eta(E)$ at one field just below the pole and several fields above it.

Fig. 2 compares the energy-dependent phase shift directly from coupled-channels calculations with that from the effective-range expansion, Eq. (2), using the accurate (field-dependent) values of r_{eff} from the previous section. The values of the effective range at the specific fields shown are given in Table II. Significant deviations can be seen for energies on the order of 1 μ K. For Cs at $B = 226.80$ G, for example, the effective-range expansion is inadequate at energies above 200 nK, corresponding to $E/\bar{E} = 2 \times 10^{-3}$. On the high-field side of the pole, there

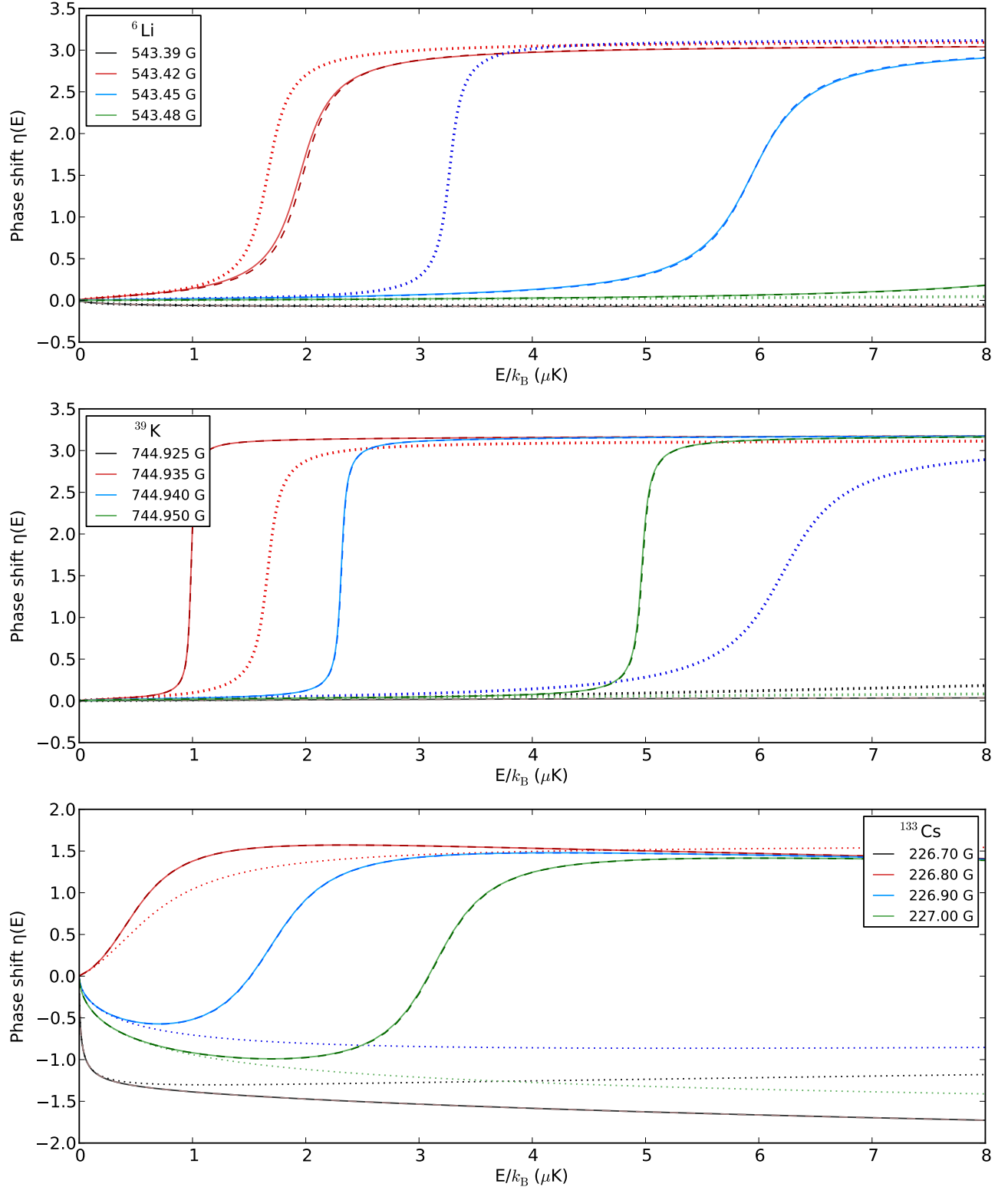


FIG. 2. Energy dependence of the phase shift $\eta(E)$ at magnetic fields around narrow resonances in ${}^6\text{Li}$, ${}^{39}\text{K}$ and ${}^{133}\text{Cs}$. Coupled-channels calculations (solid lines) give the actual variation. The effective-range expansions (dotted lines) are given by Eq. (2), except for those at 543.48 G for ${}^6\text{Li}$, 744.925 G for ${}^{39}\text{K}$, and 226.80 G for ${}^{133}\text{Cs}$, which are close to zeroes in $a_0(B)$ and are therefore calculated with the phase-shift form of Eq. (4b). The effective-range expansions deviate substantially from the coupled-channels results at collision energies on the order of μK . The MQDT approach of Section IV (dashed lines) gives an accurate representation of $\eta(E)$ over the full range of collision energies. Top: The resonance at $B_0 = 543.40$ G in the ab channel of ${}^6\text{Li}$; center: The resonance at $B_0 = 744.93$ G in the aa channel of ${}^{39}\text{K}$; bottom: The resonance at $B_0 = 226.73$ G in the aa channel of ${}^{133}\text{Cs}$.

System	\bar{a} (bohr)	B_0 (G)	Δ (G)	a_{bg} (bohr)	s_{res}	r_0 (bohr)	a_{ext} (bohr)	v (bohr ³)	$-2R^*$ (bohr)
⁶ Li	29.88		Eq. (8)	–	–	87.19	29.88	77840	–
⁶ Li	29.88	832	–262	–1593	27	87	43	-1.7×10^6	–1.1
⁶ Li	29.88	543.40	0.10	59.0	8.1×10^{-4}	–71000	60	-4.9×10^6	–74000
³⁹ K	61.77	744.93	–0.005	–33.4	6.2×10^{-4}	–190000	–34	2.2×10^6	–200000
¹³³ Cs	96.62	226.73	0.076	2062	0.19	–810	2800	1.8×10^9	–1000

TABLE I. Parameters of Eq. (11) that characterize r_{eff} in the vicinity of resonances of different types.

	B (G)	$a_0(B)$ (bohr)	r_{eff} (bohr)
${}^6\text{Li}$	543.39	456.0	-5.4×10^4
	543.42	-362.5	-9.7×10^4
	543.45	-75.3	-2.3×10^5
	543.48	-20.8	-1.1×10^6
${}^{133}\text{Cs}$	226.7	7680.6	-290
	226.8	-103.4	-4.6×10^5
	226.9	1152.2	-420
	227.0	1485.6	86
${}^{39}\text{K}$	744.925	-4.6	-7.0×10^7
	744.935	-82.0	-6.6×10^4
	744.940	-54.1	-2.7×10^4
	744.950	-43.1	-8000

TABLE II. Parameters for effective-range calculations. At each magnetic field, the zero-energy scattering length is given along with the effective range as calculated using the effective-range expansion.

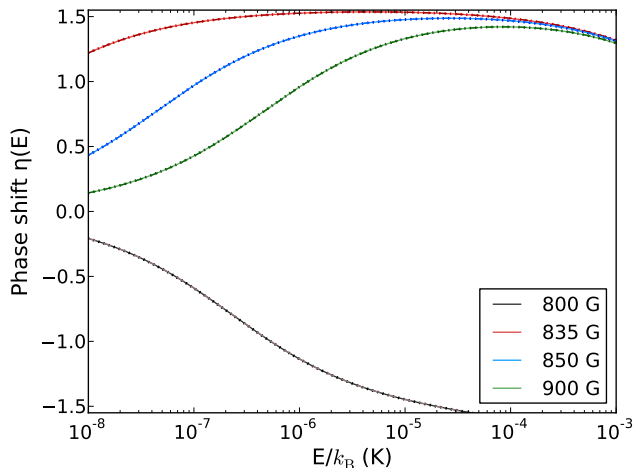


FIG. 3. Energy dependence of the phase shift, $\eta(E)$, at magnetic fields around the broad resonance in ${}^6\text{Li}$. The results of coupled-channels calculations, the effective-range expansion and the MQDT approach are indistinguishable on this scale.

is a quasibound state at low collision energy; as the energy passes through this, the phase shift η increases by π , and there is a pole in the energy-dependent phase shift $a(B)$ when $\eta(E) = \pi/2$; the location of this feature is not well captured by the effective-range expansion. This is particularly true for the Cs resonance at 226.73 G, where the non-resonant part of the phase shift has a general downwards trend as a function of energy.

We have also analysed the broad s-state resonance in ${}^6\text{Li}$ at 832 G, which has $s_{\text{res}} \gg 1$, and the results are shown in Fig. 3. In this case the effective-range expansion is indistinguishable from the results from coupled-channels calculations.

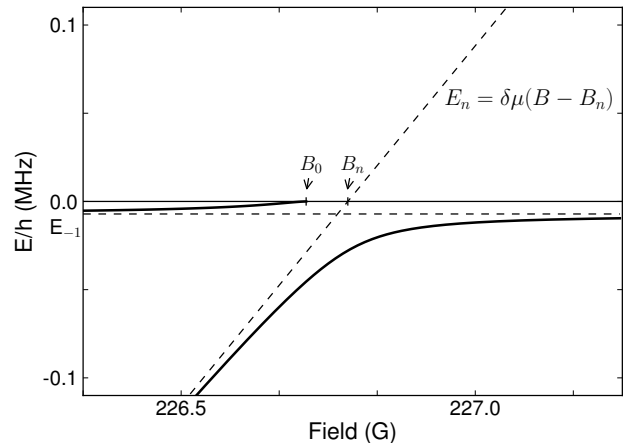


FIG. 4. The resonance at 226.73 G in the aa channel of Cs. The two-channel model (dashed lines) includes a bare bound state which crosses threshold at B_n and a reference potential whose first bound level is at E_{-1} . The bound states from the coupled-channels calculations (solid lines) have an avoided crossing with the resonance pole at B_0 .

IV. MQDT APPROACH TO AN ENERGY-DEPENDENT PHASE SHIFT

A more complete theory of the energy dependence of the phase shift may be formulated in the framework of Multichannel Quantum Defect Theory (MQDT). Julienne and Gao [32] have described a two-channel MQDT approach to resonant scattering of ultracold atoms, combining the MQDT approach of Julienne and Mies [50, 51] with the analytic van der Waals theory of Gao [29, 52–54]. A similar theory has been described by Gao [55], but in quite different notation.

For an isolated resonance, the complex set of many coupled channels can be approximated by a two-channel model where the closed channel is represented by a ‘bare’ bound state with energy E_n and the open channel by a ‘bare’ continuum state characterized by the background scattering length of the resonance. The key quantities are illustrated in Fig. 4 for the ${}^{133}\text{Cs}$ resonance near 226.73 G. The energy of the bare bound state with respect to threshold is $E_n = \delta\mu(B - B_n)$. The phase shift at fixed magnetic field follows the Breit-Wigner form, $\eta(E) = \eta_{\text{bg}} + \eta_{\text{res}}(E)$, where η_{bg} is the background component and η_{res} is the resonant component,

$$\eta_{\text{res}}(E) = -\tan^{-1} \left(\frac{\frac{1}{2}\Gamma_n}{E - E_0} \right). \quad (14)$$

Here Γ_n is the resonance width and the resonance position E_0 differs from E_n by a shift δE_n , with $E_0 = E_n + \delta E_n$. Near threshold, $\eta_{\text{bg}}(E)$, $\Gamma_n(E)$ and $\delta E_n(E)$ are strongly energy-dependent and their functional forms may be obtained from MQDT.

MQDT connects the energy-insensitive short-range potential to the energy-sensitive long-range part of the po-

tential, using the solutions for a reference potential that closely resembles the true potential at long range. The solutions for the reference potential are given at short range by WKB-normalized wavefunctions and at long range by asymptotic Bessel functions. However, at energies near threshold the WKB description breaks down at long range and the short-range solutions are connected to the long-range solutions using the MQDT functions $C(E)$ and $\tan \lambda(E)$. $C(E)$ describes the breakdown in the normalization of the WKB wavefunction at long range and scales the short-range solutions to match the long-range ones. In addition the regular and irregular WKB solutions propagated out of the short-range region lose their phase relationship, and this loss is corrected by a phase shift given by $\tan \lambda(E)$ [56]. At sufficiently high energies, the WKB wavefunctions are valid everywhere and $C(E) \rightarrow 1$ and $\tan \lambda(E) \rightarrow 0$.

The threshold behavior of the resonance width and shift may be written in terms of the MQDT functions, $C_{\text{bg}}(E)$ and $\tan \lambda_{\text{bg}}(E)$ [50, 51],

$$\frac{1}{2}\bar{\Gamma}_n(E) = \frac{1}{2}\bar{\Gamma}_n C_{\text{bg}}(E)^{-2}; \quad (15a)$$

$$\delta E_n(E) = -\frac{1}{2}\bar{\Gamma}_n \tan \lambda_{\text{bg}}(E). \quad (15b)$$

The full expression for the phase shift near a resonance is then

$$\eta(E, B) = \eta_{\text{bg}}(E) + \eta_{\text{res}}(E, B), \quad (16)$$

where

$$\eta_{\text{res}}(E, B) = -\tan^{-1} \left(\frac{\frac{1}{2}\bar{\Gamma}_n C_{\text{bg}}(E)^{-2}}{E - \delta\mu(B - B_n) + \frac{1}{2}\bar{\Gamma}_n \tan \lambda_{\text{bg}}(E)} \right) \quad (17)$$

In the present work we follow Gao's work on analytical van der Waals theory [29, 52–54, 57, 58] and choose reference functions that have the correct long-range C_6 coefficient and directly reproduce the background scattering length of the resonance. The background phase shift $\eta_{\text{bg}}(E)$ and the MQDT functions $C_{\text{bg}}^{-2}(E)$ and $\tan \lambda_{\text{bg}}(E)$ are then determined analytically by Gao's theory once the background scattering length a_{bg} is specified. The expression for $\eta_{\text{bg}}(E)$ is given by Eq. (2) of Ref. [52], and similar expressions for the other two functions have been derived and implemented numerically by Gao [59]. The energy dependence of $C_{\text{bg}}^{-2}(E)$ and $\tan \lambda_{\text{bg}}(E)$ for ^{133}Cs are shown in Fig. 5 for a variety of different a_{bg} . The threshold behavior (accurate for $ka_{\text{bg}} \ll 1$) is $C_{\text{bg}}^{-2}(E) \rightarrow k\bar{a}(1 + (a - r)^2)$ and $\tan \lambda_{\text{bg}} \rightarrow 1 - r$ as $E \rightarrow 0$ [32], where $r = a_{\text{bg}}/\bar{a}$. In this notation, $\frac{1}{2}\bar{\Gamma}_n$ is related to the magnetic resonance width Δ by

$$\frac{1}{2}\bar{\Gamma}_n = \frac{r}{1 + (1 - r)^2} \delta\mu\Delta. \quad (18)$$

To implement Eq. (17), we first carry out coupled-channel calculations of $a(B)$ and (if necessary) extrapolate to zero energy. We then fit the zero-energy scattering length to Eq. (1) to find the resonance position

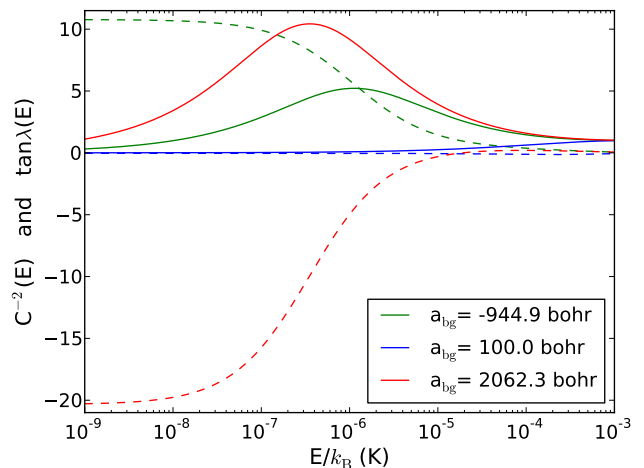


FIG. 5. The functions $C^{-2}(E)$ (solid) and $\tan \lambda(E)$ (dashed) for Cs, with a variety of different background scattering lengths. The behavior of these functions is determined by both the C_6 coefficient and the background scattering length.

B_0 , magnetic field width Δ and local a_{bg} . Along with the van der Waals coefficient C_6 and the reduced mass μ , this allows us to find the MQDT parameters $C_{\text{bg}}^{-2}(E)$ and $\tan \lambda_{\text{bg}}(E)$ using Gao's analytic van der Waals routines [59]. The shift between B_n , the crossing of the bare bound state, and the coupled-channels resonance pole B_0 is

$$B_0 - B_n = \Delta r \left(\frac{1 - r}{1 + (1 - r)^2} \right). \quad (19)$$

Lastly, we need $\delta\mu$, the difference between the magnetic moments of the bare bound state and the separated atoms. To obtain this, we carry out coupled-channels calculations on the near-threshold bound states of the system, using the approach described in ref. [60]. Such calculations give the energies of real bound states rather than bare states, but it is usually straightforward to find a region of magnetic field where the energies are only weakly perturbed by avoided crossings, and to obtain magnetic moments by finite differences in this region. If necessary, pairs of crossing states could be deperturbed to find the properties of the underlying bare states, but this was not necessary in the present work. Typically 2-3 significant figures were found to be sufficient in our calculations.

V. EFFECTIVENESS OF THE MQDT FORMULA

The MQDT formula for the energy-dependent phase shift, Eq. (17), was applied to the same set of narrow resonances discussed in Section III. The parameters obtained for the MQDT approach are given in Table III. Figure 2 compares the MQDT results with those obtained

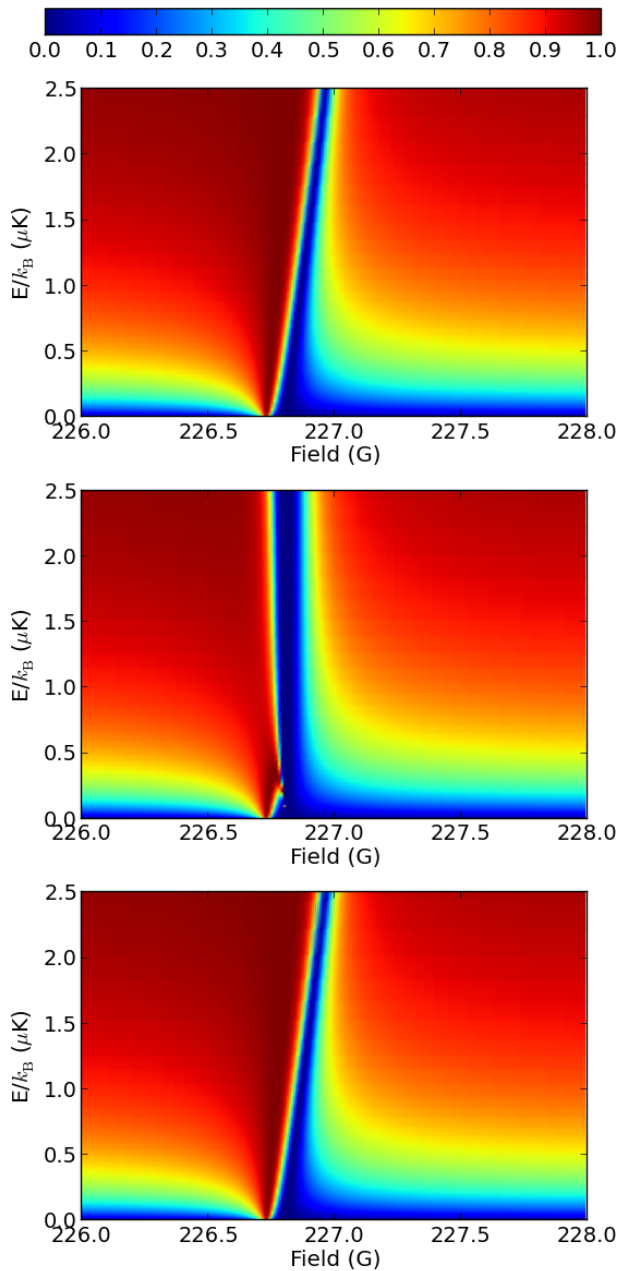


FIG. 6. Contour plot of $\sin^2 \eta(E, B)$ for $E > 0$ around the resonance at $B_0 = 226.73$ G in the aa channel of ^{133}Cs , where $E = 0$ is the energy of the two separated atoms. $\eta(E, B)$ is calculated using coupled-channels calculations (top), the effective-range expansion, Eq. (2), (middle), and the MQDT approach, Eq. (16), (bottom).

directly from coupled-channels calculations at a variety of fields around each resonance. There is excellent agreement in all cases, and MQDT succeeds in reproducing the complicated variation of the phase shift with both energy and field (which the effective-range expansion was unable to do). The MQDT approach also gives results

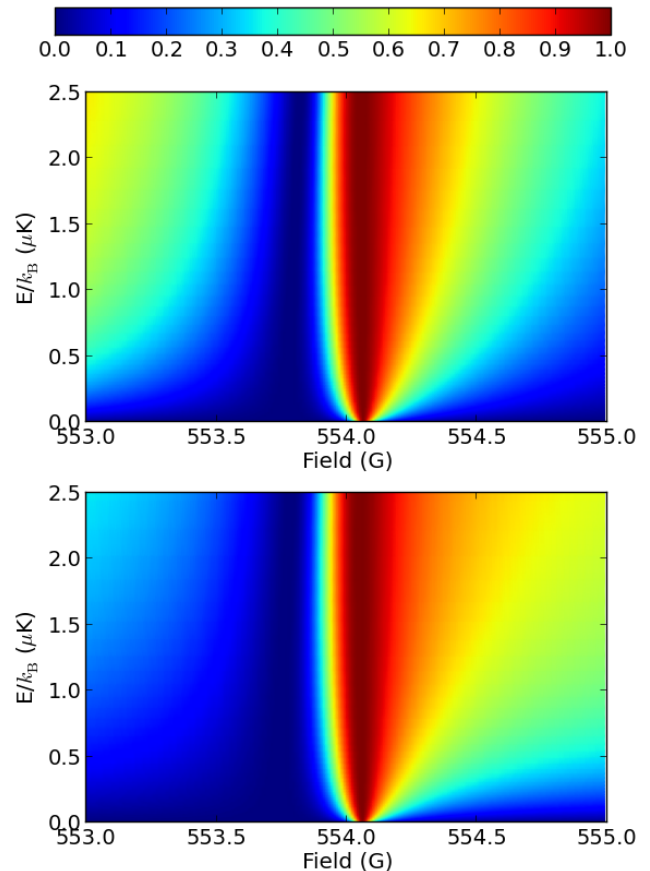


FIG. 7. Contour plot of $\sin^2 \eta(E, B)$ for $E > 0$ around the resonance at $B_0 = 554$ G in the aa channel of ^{133}Cs , where $E = 0$ is the energy of the two separated atoms. $\eta(E, B)$ is calculated using coupled-channels calculations (top) and the MQDT approach, Eq. (16), (bottom). Around the pole of the resonance where the a_{bg} fitted by the pole formula is roughly accurate then the MQDT approach works well, towards the edges of the resonance where the a_{bg} is shifted the formula breaks down.

indistinguishable from coupled-channels calculations for the broad resonance in ^6Li , shown in Fig. 3, although in this case the effective-range expansion is also successful, provided the field-dependence of r_{eff} is taken from coupled-channel calculations and not from an approximate formula.

The MQDT approach can be used to generate a smooth and accurate representation of the resonance with magnetic field both near threshold and at higher energies. Figure 6 shows contour plots of $\sin^2 \eta$ as a function of both magnetic field and energy over the width of the Cs resonance at 226.73 G, as obtained from coupled-channel calculations, from the effective range expansion and from the MQDT approach. The states that arise in the two-channel model for this resonance are shown in Fig. 4. The shift from B_0 and B_n between the dressed and bare state pictures can be clearly seen. It may be seen that the MQDT approach reproduces the coupled-channel results

System	μ (m_u)	\bar{E} (mK)	\bar{a} (bohr)	C_6 ($E_h \text{bohr}^6$)	B_0 (G)	Δ (G)	a_{bg} (bohr)	B_n (G)	$\delta\mu$ (μ_B)	s_{res}
^6Li	3.0076	32.3	29.88	1393.39	543.40	0.10	59.0	543.50	1.97	8.1×10^{-4}
^{39}K	19.4819	1.17	61.77	3926.9	745.93	-0.005	-33.4	744.93	3.95	6.2×10^{-4}
^{133}Cs	66.4527	0.14	96.62	6890.48	226.73	0.076	2062.26	226.81	0.24	0.19

TABLE III. The resonance parameters required for two-channel formula.

very accurately over the whole range of energy and field, while the effective-range expansion does not. In particular, the peak of the resonance, where $\sin^2 \eta = 1$ and $a(B) = \infty$, follows a quite incorrect path as a function of energy in the effective-range expansion.

All the calculations described above were carried out with MQDT functions that represent the ‘bare’ open channel derived from the local a_{bg} of the resonance, even if it is not the overall a_{bg} of the system. This approach works well for the examples discussed, but it is limited to resonances where a_{bg} remains reasonably constant over the width of the resonance. This is true for most resonances with $s_{\text{res}} \ll 1$, unless they sit very close to the pole of a much wider resonance; under such circumstances, however, there can be a substantial variation in a_{bg} over the width of the resonance. As an example of this we consider the resonance at $B_0 = 554$ G in the aa channel of ^{133}Cs , which is close to the pole of a broad resonance at 548 G. In Fig. 7 the energy-dependent phase shift from coupled-channels calculations is compared to the results of the MQDT approach with fixed a_{bg} . Whilst the MQDT approximation is good at fields close to the pole of the resonance, it quickly starts to fail at fields further away. This is because the two resonances need to be treated together as a pair of interfering, overlapping resonances [61] instead of treating them as independent. In such a case, the assumption of a constant background scattering length is valid only close to the resonance pole.

VI. CONCLUSION

An accurate description of the energy dependence of the scattering phase shift and hence the scattering length is crucial to many experiments on few-body phenomena at finite temperatures. We have explored the behavior of the commonly used effective-range expansion, and shown that is reasonably good at describing the energy dependence around broad resonances and away from zero-crossings in the scattering length. However, around narrow resonances the effective-range expansion can fail badly, even when the full field-dependence of the effective range is taken from coupled-channel calculations.

Gao [29] and Flambaum *et al.* [30] have developed an approximate formula relating the effective range r_{eff} to the scattering length. We have shown that this formula is reasonably accurate near the pole of a broad resonance, but even for broad resonances it breaks down badly near zero-crossings, and may give an effective range of the wrong sign. However, it is possible to write a modified

form of the formula (with a different parabolic denominator) that gives a good representation of the effective range across the whole width of the resonance. For narrow resonances, an analogous parabolic form may still be used, but its parameters are completely different from those of refs. [29] and [30].

To remedy the deficiencies of the effective-range expansion around narrow resonances, we advocate the use of an MQDT approach that fully describes the effect of a resonance as a function of both field and energy. This method entails representing the resonance in a two-channel model in which a bare bound state interacts with a bare continuum channel. The parameters of the model are obtained from coupled-channel calculations on the bound states and scattering length of the system. This MQDT approach successfully characterizes the behavior of the resonance for both broad and narrow resonances. It can be used to include the role of collision at finite energy, correct for zero-point energy in lattices, and to evaluate thermodynamic properties of cold atoms and molecules.

The MQDT approach described here is accurate only for individual isolated resonances that have a reasonably constant background scattering term across their entire width. It is not uncommon to find cases of overlapping resonances where treating individual resonances as isolated can break down to a lesser or greater extent. A full treatment of overlapping resonances would require a multi-channel treatment such as the generalized MQDT model presented by Jachymski and Julienne [61]. The energy-dependent scattering length of this model should be capable of describing the complicated variation of the scattering phase shift with energy E and magnetic field B even when there are several resonances that overlap within their widths.

Our analytic expressions for the the near-threshold energy-dependent scattering length could benefit a number of active cold atom research areas mentioned in the Introduction, since energies in the μK range are common with cold atom phenomena. This could be especially important for studies of optical lattice structures, where the finite zero-point or band energy can lead to significant corrections to the energy of confinement-induced resonances [26] and accounting for it requires the scattering length at finite energy [62, 63]. Accurate finite-energy corrections to the phase shift could also be significant for the equation of state of cold fermions [64] and for understanding few-body phenomena [21, 23].

ACKNOWLEDGMENTS

The authors are grateful to Yujun Wang for discussions. The authors acknowledge the support of EOARD

Grant FA8655-10-1-3033, AFOSR-MURI FA9550-09-1-0617, and Engineering and Physical Sciences Research Council Grant no. EP/I012044/1. CLB is supported by a Doctoral Fellowship from Durham University.

-
- [1] S. Inouye, M. R. Andrews, J. Stenger, H.-J. Miesner, D. M. Stamper-Kurn, and W. Ketterle, *Nature* **392**, 151 (1998).
- [2] S. L. Cornish, N. R. Claussen, J. L. Roberts, E. A. Cornell, and C. E. Wieman, *Phys. Rev. Lett.* **85**, 1795 (2000).
- [3] E. A. Cornell and C. E. Wieman, *Rev. Mod. Phys.* **74**, 875 (2002).
- [4] W. Ketterle, *Rev. Mod. Phys.* **74**, 1131 (2002).
- [5] T. Bourdel, L. Khaykovich, J. Cubizolles, J. Zhang, F. Chevy, M. Teichmann, L. Tarruell, S. J. J. M. F. Kokkelmans, and C. Salomon, *Phys. Rev. Lett.* **93**, 050401 (2004).
- [6] M. W. Zwierlein, C. A. Stan, C. H. Schunck, S. M. F. Raupach, A. J. Kerman, and W. Ketterle, *Phys. Rev. Lett.* **92**, 120403 (2004).
- [7] M. Inguscio, W. Ketterle, and C. Salomon, eds., *Ultracold Fermi Gases* (IOS Press, Amsterdam, 2008) Proceedings of the International School of Physics “Enrico Fermi”, Course CLXIV, Varenna, 20-30 June 2006.
- [8] S. Jochim, M. Bartenstein, A. Altmeyer, G. Hendl, C. Chin, J. Hecker Denschlag, and R. Grimm, *Phys. Rev. Lett.* **91**, 240402 (2003).
- [9] K.-K. Ni, S. Ospelkaus, M. H. G. de Miranda, A. Pe’er, B. Neyenhuis, J. J. Zirbel, S. Kotochigova, P. S. Julienne, D. S. Jin, and J. Ye, *Science* **322**, 231 (2008).
- [10] F. Lang, K. Winkler, C. Strauss, R. Grimm, and J. Hecker Denschlag, *Phys. Rev. Lett.* **101**, 133005 (2008).
- [11] M. Greiner and S. Fölling, *Nature* **453**, 736 (2008).
- [12] I. Bloch, *Nature Phys.* **1**, 23 (2005).
- [13] Y. Wang and B. D. Esry, *New J. Phys.* **13**, 035025 (2011).
- [14] S. Roy, M. Landini, A. Trenkwalder, G. Semeghini, G. Spagnolli, A. Simoni, M. Fattori, M. Inguscio, and G. Modugno, *Phys. Rev. Lett.* **111**, 053202 (2013).
- [15] F. Ferlaino, A. Zenesini, M. Berninger, B. Huang, H. Nägerl, and R. Grimm, *Few-Body Systems* **51**, 113 (2011).
- [16] M. Berninger, A. Zenesini, B. Huang, W. Harm, H.-C. Nägerl, F. Ferlaino, R. Grimm, P. S. Julienne, and J. M. Hutson, *Phys. Rev. Lett.* **107**, 120401 (2011).
- [17] A. J. Moerdijk, B. J. Verhaar, and A. Axelsson, *Phys. Rev. A* **51**, 4852 (1995).
- [18] H. A. Bethe, *Phys. Rev.* **76**, 38 (1949).
- [19] O. Hinkelmann and L. Spruch, *Phys. Rev. A* **3**, 642 (1971).
- [20] J. M. Hutson, *New J. Phys.* **9**, 152 (2007).
- [21] E. Braaten and H.-W. Hammer, *Phys. Rep.* **428**, 259 (2006).
- [22] D. Blume, *Rep. Prog. Phys.* **75**, 046401 (2012).
- [23] Y. Wang, J. P. D’Incao, and B. D. Esry, *Adv. At., Mol., Opt. Phys.* **62**, 1 (2013).
- [24] Y. Wang, J. P. D’Incao, and C. H. Greene, *Phys. Rev. Lett.* **107**, 233201 (2011).
- [25] P. Dyke, S. E. Pollack, and R. G. Hulet, *Phys. Rev. A* **88**, 023625 (2013).
- [26] P. Naidon, E. Tiesinga, W. F. Mitchell, and P. S. Julienne, *New J. Phys.* **9**, 19 (2007).
- [27] F. H. Mies and P. S. Julienne, *J. Chem. Phys.* **77**, 6162 (1982).
- [28] N. T. Zinner and M. Thogersen, *Phys. Rev. A* **80**, 023607 (2009).
- [29] B. Gao, *Phys. Rev. A* **58**, 4222 (1998).
- [30] V. V. Flambaum, G. F. Gribakin, and C. Harabati, *Phys. Rev. A* **59**, 1998 (1999).
- [31] B. Gao, *Phys. Rev. A* **84**, 022706 (2011).
- [32] P. S. Julienne and B. Gao, *AIP Conference Proceedings* **869**, 261 (2006).
- [33] P. Naidon and M. Ueda, *C. R. Phys.* **12**, 13 (2011).
- [34] E. Braaten, H. W. Hammer, D. Kang, and L. Platter, *Phys. Rev. A* **81**, 013605 (2010).
- [35] T. B. Ottenstein, T. Lompe, M. Kohnen, A. N. Wenz, and S. Jochim, *Phys. Rev. Lett.* **101**, 203202 (2008).
- [36] J. H. Huckans, J. R. Williams, E. L. Hazlett, R. W. Stites, and K. M. O’Hara, *Phys. Rev. Lett.* **102**, 165302 (2009).
- [37] M. Zaccanti, B. Deissler, C. D’Errico, M. Fattori, M. Jona-Lasinio, S. Muller, G. Roati, M. Inguscio, and G. Modugno, *Nat. Phys.* **5**, 586 (2009).
- [38] T. Kraemer, M. Mark, P. Waldburger, J. G. Danzl, C. Chin, B. Engeser, A. D. Lange, K. Pilch, A. Jaakkola, H. C. Nägerl, and R. Grimm, *Nature* **440**, 315 (2006).
- [39] G. Zürn, T. Lompe, A. N. Wenz, S. Jochim, P. S. Julienne, and J. M. Hutson, *Phys. Rev. Lett.* **110**, 135301 (2013).
- [40] M. Berninger, A. Zenesini, B. Huang, W. Harm, H.-C. Nägerl, F. Ferlaino, R. Grimm, P. S. Julienne, and J. M. Hutson, *Phys. Rev. A* **87**, 032517 (2013).
- [41] S. Falke, H. Knöckel, J. Friebe, M. Riedmann, E. Tiemann, and C. Lisdar, *Phys. Rev. A* **78**, 012503 (2008).
- [42] C. Chin, R. Grimm, E. Tiesinga, and P. S. Julienne, *Rev. Mod. Phys.* **82**, 1225 (2010).
- [43] G. F. Gribakin and V. V. Flambaum, *Phys. Rev. A* **48**, 546 (1993).
- [44] J. M. Hutson and S. Green, “MOLSCAT computer program, version 14,” distributed by Collaborative Computational Project No. 6 of the UK Engineering and Physical Sciences Research Council (1994).
- [45] J. M. Hutson, “FIELD computer program, version 1,” (2011).
- [46] D. E. Manolopoulos, *J. Chem. Phys.* **85**, 6425 (1986).
- [47] M. H. Alexander, *J. Chem. Phys.* **81**, 4510 (1984).
- [48] D. S. Petrov, *Phys. Rev. Lett.* **93**, 143201 (2004).
- [49] G. M. Bruun, A. D. Jackson, and E. E. Kolomeitsev, *Phys. Rev. A* **71**, 052713 (2005).
- [50] F. H. Mies, *J. Chem. Phys.* **80**, 2514 (1984).
- [51] F. H. Mies and P. S. Julienne, *J. Chem. Phys.* **80**, 2526 (1984).
- [52] B. Gao, *Phys. Rev. A* **62**, 050702 (2000).
- [53] B. Gao, *Phys. Rev. A* **64**, 010701 (2001).
- [54] B. Gao, *J. Phys. B* **37**, 4273 (2004).

- [55] B. Gao, *Phys. Rev. A* **78**, 012702 (2008).
- [56] P. S. Julienne and F. H. Mies, *J. Opt. Soc. Am. B* **6**, 2257 (1989).
- [57] B. Gao, *Phys. Rev. A* **58**, 1728 (1998).
- [58] B. Gao, *Phys. Rev. Lett.* **83**, 4225 (1999).
- [59] B. Gao, "Routines to calculate the AQDT parameters for an attractive $1/r^6$ potential, Version 2," (2003), University of Toledo, Ohio.
- [60] J. M. Hutson, E. Tiesinga, and P. S. Julienne, *Phys. Rev. A* **78**, 052703 (2008).
- [61] K. Jachymski and P. S. Julienne, *Phys. Rev. A* **88**, 052701 (2013).
- [62] D. Blume and C. H. Greene, *Phys. Rev. A* **65**, 043613 (2002).
- [63] E. L. Bolda, E. Tiesinga, and P. S. Julienne, *Phys. Rev. A* **66**, 013403 (2002).
- [64] X.-J. Liu, *Phys. Rep.* **524**, 37 (2013).